Quantifying the biophysical characteristics of *Plasmodium-falciparum*-parasitized red blood cells in microcirculation

D. A. Fedosov[a,b], B. Caswell[a], S. Suresh[c], and G. E. Karniadakis[a,1]

[a]Division of Applied Mathematics, Brown University, Providence, RI 02912; [c]Department of Materials Science and Engineering, Massachusetts Institute of Technology, Cambridge, MA 02139; and [b]Institut für Festkörperforschung, Forschungszentrum Jülich, 52425 Jülich, Germany

Edited by Robert H. Austin, Princeton University, Princeton, NJ, and approved November 15, 2010 (received for review July 2, 2010)

The pathogenicity of *Plasmodium falciparum* (*Pf*) malaria results from the stiffening of red blood cells (RBCs) and its ability to adhere to endothelial cells (cytoadherence). The dynamics of Pf-parasitized RBCs is studied by three-dimensional mesoscopic simulations of flow in cylindrical capillaries in order to predict the flow resistance enhancement at different parasitemia levels. In addition, the adhesive dynamics of *Pf*-RBCs is explored for various parameters revealing several types of cell dynamics such as firm adhesion, very slow slipping along the wall, and intermittent flipping. The parasite inside the RBC is modeled explicitly in order to capture phenomena such as "hindered tumbling" motion of the RBC and the sudden transition from firm RBC cytoadherence to flipping on the endothelial surface. These predictions are in quantitative agreement with recent experimental observations, and thus the three-dimensional modeling method presented here provides new capabilities for guiding and interpreting future in vitro and in vivo studies of malaria.

adhesion | erythrocyte | malaria | mechanical properties | dissipative particle dynamics

Red blood cells parasitized by *Plasmodium falciparum* (*Pf*-RBCs) undergo irreversible changes in structure and biophysical characteristics, which can lead to drastically altered blood circulation. The membrane shear modulus of infected RBCs may increase up to ten-fold causing capillary occlusions (1, 2), thereby resulting in substantial increase in resistance to blood flow. Such effects may be intensified due to the enhanced cytoadherence of *Pf*-RBCs to the vascular endothelium (3–6). This adherence of *Pf*-RBCs is believed to be the main cause of bleeding complications in cerebral malaria due to blockages of small vessels in the brain (7). Unlike the extensive research on leukocytes, very few in vitro experiments (8–11) have examined the adhesive dynamics of *Pf*-RBCs. For example, in ref. 8 the walls of microfluidic channels were coated with purified protein ligands participating in cytoadherence (e.g., ICAM-1) and with mammalian Chinese hamster ovary (CHO) cells expressing such ligands. Purified ICAM-1 caused rolling or flipping of *Pf*-RBCs without detachment or arrest of RBC motion. In contrast, mammalian CHO cells seem to result mostly in a firm attachment of *Pf*-RBCs with sporadic complete detachment. This difference in behavior and the complicated adhesive dynamics of *Pf*-RBCs have not been studied quantitatively. More broadly, there have not been any quantitative studies of the dynamics of RBCs in malaria to investigate the rheology and flow resistance in addition to the reported new adhesive dynamics.

Recent progress in multiscale numerical modeling (12–14) allows us to model soft matter, and RBCs in particular, at sufficient detail, i.e., simulating nanometer scales while simultaneously capturing the large scale dynamics. We have developed and validated a Dissipative Particle Dynamics (DPD) model (12, 14–16) that can accurately simulate the properties and dynamic behavior of healthy RBCs as well as *Pf*-RBCs. The multiscale model can represent a RBC at the spectrin level with 30,000 points (17) or at a coarser level with 500 points by proper scaling of the physiologically correct parameters (12, 14, 15); hence, no ad hoc calibration is required. The predictive capability of the DPD model has been demonstrated in comparisons with microfluidic experiments that probe controlled pressure-velocity relationships of (healthy) RBC flow through microchannels whose inner openings mimic the smallest dimensions for RBC passage in the microvasculature (16). In addition, we have extended the adhesive dynamics model of (18, 19) to the DPD framework, and validated it by simulating the adhesive dynamics of leukocytes for which extensive experimental results exist (20, 21). In summary, in the current work using DPD we model the RBC membrane as a viscoelastic material, the solid *Pf*-parasite, the fluid inside the cells and the exterior plasma, as well as the functionalized microchannel walls. The model parameters include the membrane shear modulus μ_0, the membrane bending rigidity k_c, the membrane viscosity η_m, and the interior/exterior η_i/η_o fluid viscosities; see *Methods* and *SI Text* for more details.

Results

We first validate our RBC model in health and disease with physiologically correct values of all parameters using data from optical tweezers experiments. Subsequently, using the *same* set of parameters we investigate the dynamics of *Pf*-RBCs at different parasitemia levels and quantify the different modes of adhesive dynamics in the presence of ICAM-1 coated wall surfaces.

Increased Stiffness of *Pf*-Parasitized RBCs. In malaria disease, progression through the parasite development stages (ring → trophozoite → schizont) leads to a considerable stiffening of *Pf*-RBCs compared to healthy ones (22, 23). Furthermore, in the schizont stage the RBC shape becomes near-spherical whereas in the preceding stages RBCs maintain their biconcavity. Fig. 1 shows simulation results for healthy RBCs and *Pf*-RBCs at different stages of parasite development compared with optical tweezers experiments (23). The simulation results were obtained with a stress-free multiscale RBC model (see *Methods*) with 500 points, shear modulus $\mu_0 = 6.3$ μN/m for the healthy RBC, 14.5 for the ring stage, 29 for the trophozoite, and 60 μN/m for the schizont; these values are consistent with the experiments of refs. 22, 23. The bending rigidity for all cases is set to 2.4×10^{-19} J, which is the value of bending rigidity for healthy RBCs, as the membrane bending stiffness for different stages is not known. The curve for the schizont stage marked as "near-spherical" corresponds to stretching an ellipsoidal shape with

Author contributions: B.C., S.S., and G.E.K. designed research; D.A.F. performed research; D.A.F. analyzed data; and D.A.F., B.C., S.S., and G.E.K. wrote the paper.

The authors declare no conflict of interest.

This article is a PNAS Direct Submission.

[1]To whom correspondence should be addressed. E-mail: gk@dam.brown.edu.

This article contains supporting information online at www.pnas.org/lookup/suppl/doi:10.1073/pnas.1009492108/-/DCSupplemental.

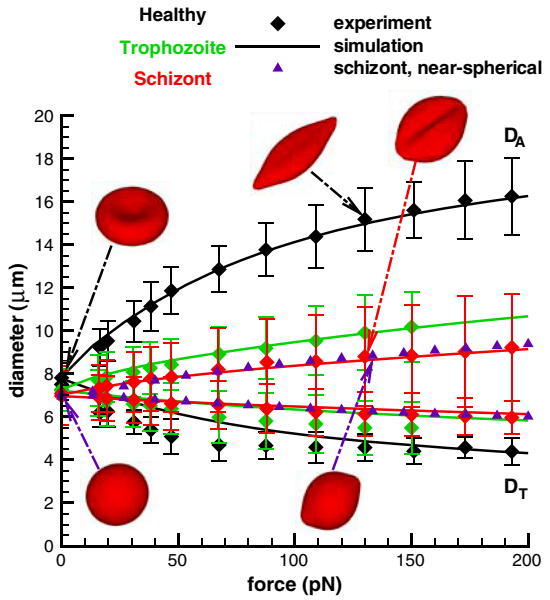

Fig. 1. Increased stiffening of *Pf*-RBCs: Simulated stretching of healthy and *Pf*-RBCs at different malaria stages compared with optical tweezers experiments (23). D_A and D_T refer to the axial and transverse diameters.

axes $a_x = a_y = 1.2a_z$. Here, the membrane shear modulus of 40 μN/m matches the stress-strain response with the experiment, i.e., it is smaller than that for the biconcave-shape simulation. For the near-spherical cell the membrane is subject to stronger local stretching for the same uniaxial deformation compared to the biconcave shape. For the deflated biconcave shape, the inner fluid volume can be deformed in response to stretching, while in the near-spherical shape the fluid volume applies additional resistance onto the stretched membrane. Hence, the cell geometry plays an important role, and hence it has to be closely modeled for accurate extraction of parameters from the optical tweezers experiments. In all simulations that follow we used the biconcave RBC shape.

Flow Resistance. First we model the blood as a suspension of healthy RBCs using the DPD model and simulate blood flow in tubes of diameters ranging from 10 μm to 40 μm. It is important to model carefully the excluded volume (EV) interactions among cells, which are often implemented through a repulsive force between membrane vertices of different cells. A certain range (i.e., force cutoff radius) of the repulsive interactions may impose a nonzero minimum distance between neighboring RBC membranes, the so-called "screening distance" between membranes. The choice of a smaller cutoff radius may result in overlapping of cells, while a larger value would increase the screening distance between cells. This distance may be unphysical and may strongly affect the results at high volume fractions of RBCs. A better approach is to enforce EV interactions among cells by employing reflections of RBC vertices on the membrane surfaces of other cells yielding essentially a zero screening distance between two RBC surfaces. In addition, we employ a *net repulsion* of RBCs from the wall by properly setting the repulsive force coefficient between the wall particles and the cell vertices.

RBCs in Poiseuille flow migrate to the tube center forming a core in the flow. Fig. 2 shows a sample snapshot of RCBs flowing in a tube of diameter $D = 20$ μm. The pressure gradients employed here are 2.633×10^5, 1.316×10^5, and 6.582×10^4 Pa/m for tubes of diameters 10, 20, and 40 μm, respectively. In the case of low hematocrit H_t (e.g., 0.15) the velocity profiles closely follow parabolic curves in the near-wall region. In the central region of the tube a substantial reduction in velocity is found

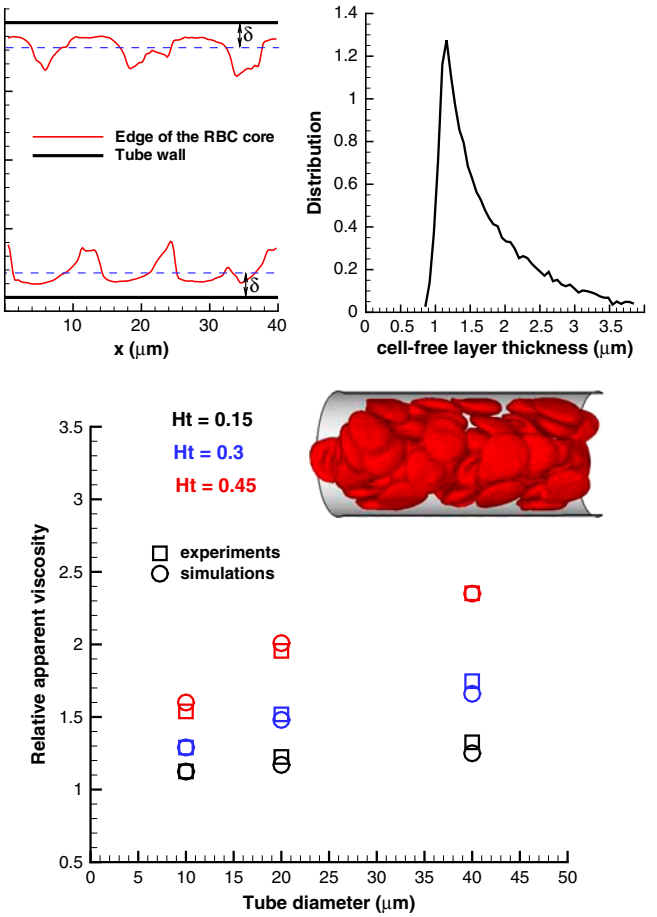

Fig. 2. Flow resistance in health: Upper: An example of a CFL edge (left) and local CFL thickness distribution (right) for $H_t = 0.45$ and $D = 20$ μm. Lower: Relative apparent viscosity in comparison with experimental data (26) for various H_t values and tube diameters. Inset plot is a snapshot of RCBs in Poiseuille flow in a tube of a diameter $D = 20$ μm at $H_t = 0.45$.

for all volume fractions in comparison with the parabolic profiles indicating a decrease in the flow rate (15). A RBC core formation is established with a thin plasma layer next to the tube walls called the *cell-free* layer (CFL) (15). The thickness of the CFL is directly related to the Fahraeus and the Fahraeus-Lindqvist effects, both of which were accurately simulated by our DPD model (15). To determine the CFL thickness we computed the outer edge of the RBC core, which is similar to CFL measurements in experiments (24, 25). Fig. 2 shows a sample CFL edge from simulations for $H_t = 0.45$ and $D = 20$ μm and local CFL thickness distribution, which is constructed from a set of discrete local measurements of CFL thickness taken every 0.5 μm along the flow (x) direction. The fluid viscosity of the CFL region is much smaller than that of the tube core populated with RBCs providing an effective lubrication for the core to flow. The apparent viscosity is defined as follows $\eta_{\text{app}} = \frac{\pi \Delta P D^4}{128 Q L}$, where ΔP is the pressure difference, Q is the flow rate, and L is the length of the tube. The apparent viscosity increases for higher H_t values because higher cell crowding yields larger flow resistance. It is more convenient to consider the relative apparent viscosity defined as $\eta_{\text{rel}} = \frac{\eta_{\text{app}}}{\eta_s}$, where η_s is the solvent viscosity. Fig. 2 shows the simulated η_{rel} values in comparison with the empirical fit to experiments (26) for the tube diameter range 10–40 μm and H_t values in the range 0.15–0.45. Excellent agreement between simulations and experiments is obtained for the proper EV interactions for all cases tested.

Next we simulate blood flow in malaria as a suspension of healthy and *Pf*-RBCs at the trophozoite stage and hematocrit

$H_t = 0.45$. Several parasitemia levels (percentage of *Pf*-RBCs with respect to the total number of cells in a unit volume) from 5% to 100% are considered in vessels with diameters 10 and 20 μm. The inset of Fig. 3 shows a snapshot of RCBs flowing in a tube of diameter 20 μm at a parasitemia level of 25%, see also Movie S1. The main result in Fig. 3 is given by the plot of the relative apparent viscosity in malaria—a measure of flow resistance—obtained at different parasitemia levels. The effect of parasitemia level appears to be more prominent for small diameters and high H_t values. Thus, at $H_t = 0.45$ blood flow resistance in malaria may increase up to 50% in vessels of diameters around 10 μm and up to 43% for vessel diameters around 20 μm. These increases do not include any contributions from the interaction of *Pf*-RBCs with the glycocalyx (27, 28); such important interactions are complex as they may include cytoadhesion which we model next.

Adhesive Dynamics. The adhesive dynamics of *Pf*-RBCs in shear flow was studied for different values of wall shear stress (WSS) and compared with the experiments of ref. 8 for the wall coated with purified ICAM-1. Fig. 4 (upper left) shows several successive snapshots of a simulated cell rolling along the wall. Small blue particles are added as tracers for visual clarity, and distinct RBC snapshots are separated by shifting their x coordinate. The dynamics of the *Pf*-RBCs is characterized by a flipping behavior initiated at first by the cell peeling off the wall due to the hydrodynamic force after flat RBC adhesion (the first snapshot in the plot; see also Movie S2). After most of the initial cell wall contact area is peeled off, the RBC flips over onto its other side facilitated by the remaining small wall contact area. During these steps, *Pf*-RBCs undergo large membrane deformations as illustrated in the plot and in Movie S2. Similar flipping behavior and large membrane deformations (including membrane buckling) were also found in the experiments (8).

WSS appears to be the key parameter governing the *Pf*-RBC adhesive dynamics, because adhered RBCs are driven by fluid stresses and roll along the wall with a much smaller velocity than the flow velocity. Several initial simulations with varying WSS and other parameters fixed revealed that *Pf*-RBCs may exhibit firm adhesion at a WSS lower than 0.317 Pa while they can completely detach from the wall at higher values. Systematic visualizations

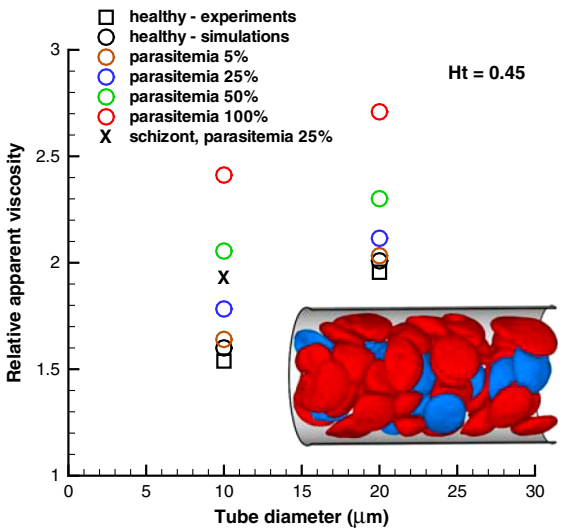

Fig. 3. Flow resistance in malaria: Healthy (red) and *Pf*-RBCs (blue) in Poiseuille flow in a tube of diameter $D = 20$ μm. $H_t = 0.45$, parasitemia level 25%. Plotted is the relative apparent viscosity of blood in malaria for various parasitemia levels and tube diameters. Symbol "x" corresponds to the schizont stage with a near-spherical shape. Experimental data from the empirical fit by Pries et al. (26).

showed that *Pf*-RBC detachment at high WSS occurs during the relatively fast motion of RBC flipping, because the contact area is then minimal. However, in the experiments of ref. 8 *Pf*-RBCs moved on a surface coated with purified ICAM-1 showing persistent and stable rolling over long observation times for a wide range of WSS between 0.2 Pa and 2 Pa. This observation suggests a stabilizing mechanism for the rolling of *Pf*-RBCs at high shear stresses. Such behavior is not surprising because it is known that leukocyte adhesion can be actively regulated with flow conditions and with biochemical stimuli (29, 30).

To stabilize RBC binding at high shear stresses we need to improve the model by allowing the bond spring constant (k_s) to vary with WSS; here, for simplicity we assume linear dependence of k_s on WSS. Fig. 4 (lower left) presents the average rolling velocity of *Pf*-RBCs compared with experiments of cell rolling on a surface coated with purified ICAM-1 (8). The simulated average velocities show a near-linear dependence on the shear stress, and are in good agreement with the experiments. The discrepancy at the highest simulated shear stress suggests a further strengthening of cell-wall bond interactions. However, the simulated values remain between the 10th and the 90th percentiles found in experiments.

In general, the adhesive behavior of *Pf*-RBCs, explored by means of numerical simulation for various parameters, revealed several types of cell dynamics such as firm adhesion, RBC peeling off the surface followed by flipping from one side to the other or by detachment from the wall, and very slow slipping along the wall. However, close examination of the video containing an example of RBC adhesive dynamics on the mammalian CHO cells from experiments (8) shows firm adhesion of *Pf*-RBCs for some time followed by *sudden* detachment. In contrast, firm adhesion in simulations appears always to be stable with no detachment within the simulation time of approximately 30 s. In experiments the *Pf*-RBC motion before the detachment displays very slow slipping along the surface due to the flow and random collisions with other flowing RBCs. Hence, it is likely that the sudden complete detachment from the wall is caused by the RBC slipping into a wall region with a limited number of ligands available for binding due to imperfect coating. To verify this hypothesis we ran a simulation in which the ligand sites were removed from the wall area between 30 μm and 40 μm in the flow direction. Fig. 4 (lower right) presents the *Pf*-RBC instantaneous velocity (green curve) corresponding to slow slipping along the surface continued up to an x coordinate (stream-wise position) between 30 μm and 40 μm, where a complete cell detachment occurs due to absence of ligands for binding, in agreement with the *Pf*-RBC dynamics on the mammalian CHO cells found in experiments (8). No other change in physical parameters of cell adhesion have been found to reproduce these dynamics.

Next, we model explicitly the effect of the solid parasite inside the *Pf*-RBCs. Recent experiments (22) suggest that the volume of cytosol may be reduced threefold in the later stages of intracell parasite development compared to healthy RBCs, indicating that the parasite takes up considerable volume within a *Pf*-RBC. Hence, a sufficiently large parasite provides a rigid backbone within a *Pf*-RBC to strongly affect its adhesive dynamics. In experiments in ref. 9 it was observed that the parasite is attached to one side, especially in the ring and trophozoite stages, causing a structural anisotropy in the *Pf*-RBC that affects cytoadherence. The parasite is modeled as a collection of DPD particles uniformly distributed within a cylindrical volume of radius 3.3 μm and height 0.2 μm. These particles are placed inside the modeled RBC and constrained to undergo rigid motion. To prevent the parasite body from crossing the RBC membrane, we introduce Lennard-Jones interactions between the parasite body particles and membrane vertices; however, the parasite swims freely in the RBC cytosol. The number of DPD particles to represent the RBC cytosol is reduced according to the volume occupied by the

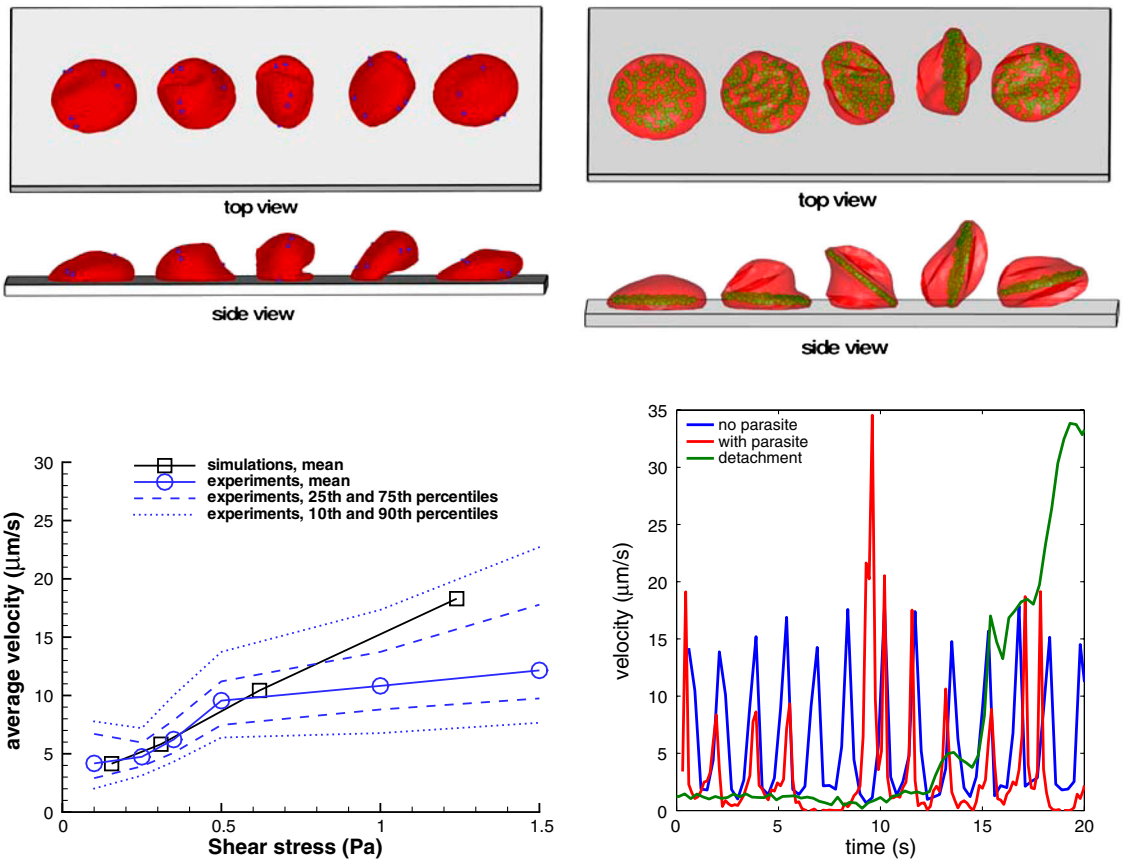

Fig. 4. Adhesive dynamics: Upper left: Top and side views of successive snapshots of a single flipping of an infected RBC; see also Movie S2. Upper right: Top and side views of several snapshots of a rolling RBC with a parasite body inside the cell (drawn in green); see also Movie S3. Lower left: Average rolling velocity of infected RBCs depending on the shear stress compared with the experiments of cell rolling on purified ICAM-1 (8). Experimental data include mean values and curves that correspond to the 10th, 25th, 75th, and 90th percentiles. Lower right: Velocities of *Pf*-RBCs with/without parasitic body, and for the case of complete detachment.

parasite body. Fig. 4 (upper right) presents successive snapshots of a rolling RBC with a rigid parasite inside the cell (see also Movie S3). The RBC membrane displays local buckling due to its low bending rigidity, which is consistent with the RBC visualizations in Fig. 4 (upper left). In addition, a "hindered tumbling" motion of the membrane appears to be caused by the solid parasite, see Movie S3. Fig. 4 (lower right) shows the corresponding instantaneous velocity (red curve), exhibiting a more erratic pattern than the blue curve. For example, the red curve in Fig. 4 (lower right) indicates several time intervals during which the *Pf*-RBC shows firm adhesion for several seconds. Furthermore, firm adhesion may be followed by several fast flips of the RBC along the surface characterized by two closely located peaks of velocity around the time of 20 s. Systematic visualizations revealed that the smaller peaks of cell velocity in Fig. 4 (lower right) correspond to "hindered tumbling" motion facilitated by the parasite body due to the parasite being freely suspended in the RBC cytosol. A proper positioning of the parasite body inside the RBC may result in a stress distribution on the front part of the membrane which forces the RBC into a crawling motion.

Discussion

We have employed a validated multiscale model to quantify the dynamic properties of *Pf*-RBCs in typical conditions encountered in the microcirculation. Specifically, the simulated mechanical responses of healthy RBCs and *Pf*-RBCs were found to be in excellent agreement with optical tweezers experiments as did the dynamic responses measured in terms of the cell-free layer and the increase in the apparent blood viscosity. Flow resistance was computed at parasitemia levels higher than those often found in clinical blood tests (31) of individuals suffering from malaria. At a parasitemia level above 0.2% an immune response is initiated, and levels around 20% are found in very severe cases of malaria with high mortality (9, 32). Clinical tests are able to detect *Pf*-RBCs at a parasitemia level as small as 0.0001–0.0004%. Active malaria in most cases is characterized by levels of 0.5%–20%. Even though the parasitemia levels simulated here are beyond this range, we attempted to span the full range 0%–100% to evaluate the dependence of blood flow properties on parasitemia levels. At low parasitemia levels, differences in measured properties may not be significant, and therefore they would be difficult to detect. It is also possible that the predicted resistance in simulations is underestimated due to a potential increase in membrane bending rigidity of *Pf*-RBCs and the presence of "rigid" parasites inside the cells. These properties of Pf-RBCs could further impair the ability of *Pf*-RBCs to comply with deformations in the flow, and consequently prevent their close packing in the flow core. Other conditions, not considered here, are more likely to significantly influence blood flow resistance in malaria. For example, stiffer *Pf*-RBCs can block small capillaries up to 5–6 μm in diameter (1). In addition, the property of *Pf*-RBCs to adhere to each other and to vascular endothelium at later stages of parasite development may strongly impair blood flow in capillaries and small arterioles resulting in a substantial increase of flow resistance.

The dependence of the RBC rolling velocity on shear stress found in experiments is clearly nonlinear. Therefore, the assumption of linear dependence of k_s on the shear stress is an oversimplification. In addition, there may be a change in bond association and dissociation kinetics with shear stress, which would affect the rolling stabilization of infected RBCs at high shear rates. Our simulations suggest that the adhesive dynamics of *Pf*-RBCs is not sensitive to changes below 30%–40% in reaction rates k_{on}^0 and k_{off}^0. However, the cell dynamics may be strongly affected if these parameters are changed considerably as seen in leukocyte dynamics simulations. Moreover, experimental data show a broader scatter of the average RBC velocity for different cells than found in simulations (15). This observation is likely to be related to nonuniform distributions of receptors on the RBC

membrane and ligands on the wall. In the simulations, distributions of both receptors and ligands are fixed, and are nearly homogeneous with approximately the same area occupied by each receptor or each ligand. A scatter in behavior among distinct RBCs in the simulations is solely related to the stochastic nature of the adhesive model. However, in experiments irregular distributions of receptors and ligands are likely to significantly contribute to scatter in RBC adhesive dynamics.

The parasite body constrains the RBC membrane by supplying a rigid support, which forces RBC flipping without substantial bending. The presence of a rigid body inside a RBC significantly affects the RBC adhesive dynamics resulting in behavior more erratic compared with the more regular adhesive dynamics of RBCs with no parasites. A thin disk to represent the parasite body was considered; however, other geometrical forms or sizes of the parasite may have a different effect on RBC adhesive dynamics. Therefore, an experimental characterization of the parasite geometry for different stages of parasite development would be of great interest. In addition, the modeled parasite body was freely suspended in the RBC cytosol, while under real conditions it is likely that the parasite is attached to the membrane, because it exposes adhesive proteins on the membrane surface to mediate binding to the wall. These unresolved issues require further experimental and numerical investigation.

Methods

Simulation Method. The DPD method (33) is a particle-based mesoscopic simulation technique, where a simulated system consists of N point particles. Each particle corresponds to a *collection* of atoms or molecules rather than an individual atom. DPD particles interact through pair wise soft potentials and move according to the Newton's second law of motion; see also *SI Text*.

Membrane Model. The RBC membrane is modeled by 500 discrete points, which are the vertices of a triangular network of springs on the membrane surface. Such network models have been used extensively to simulate membranes, e.g., see ref. 34. The network of fixed connectivity provides the elastic and the viscous response of a RBC because a "dashpot" is attached to each spring. The RBC model also includes bending energy between neighboring triangular plaquettes and area and volume constraints. We use a "stress-free" model (14, 15) which eliminates artifacts of irregular triangulation. The ''stress-free'' model is obtained by simulation annealing such that each spring assumes its own equilibrium spring length adjusted to be the edge length after triangulation. RBC-fluid boundary conditions are enforced through bounce-back reflections of fluid particles on the membrane triangles and by a proper setting of interactions between fluid particles and RBC vertices. More details on the RBC model can be found in the *SI Text*.

Adhesive Dynamics. Adhesive dynamics is simulated with the stochastic bond formation/dissociation model similar to ref. 18. The bonds are modeled as linear springs and their formation k_{on} and dissociation k_{off} rates depend on the separation distance between the RBC receptors and ligands distributed on the wall as a square lattice with the lattice constant of 0.5 μm. The receptor and ligand densities in simulations may be different from those in experiments (8). However, we note that receptor-ligand interactions in simulations correspond to effective adhesive interactions of *Pf*-RBCs with the wall. The simulated receptor-ligand interactions do not correspond to actual molecular bonds and may represent a number of existing molecular bonds. Adhesive dynamics in simulations proceeds by: (*i*) checking for potential dissociation of existing bonds with probability $1 - \exp(-k_{off}\Delta t)$, where Δt is the time step, (*ii*) testing unbound ligands for potential bond formation with probability $1 - \exp(-k_{on}\Delta t)$, and (*iii*) applying forces of all existing bonds. More details on the adhesive dynamics and model parameters can be found in *SI Text*.

ACKNOWLEDGMENTS. We thank the anonymous referees for their helpful suggestions. This work was supported by the National Institutes of Health (NIH) Grant R01HL094270. G.E.K. acknowledges support from the National Science Foundation (NSF) Grant CBET-0852948. S.S. acknowledges support from the Interdisciplinary Research Group on Infectious Diseases (ID), which is funded by the Singapore-Massachusetts Institute of Technology (MIT) Alliance for Research and Technology (SMART). Computations were performed at the NSF's National Institute for Computational Sciences at University of Tennessee (NICS) facility.

1. Shelby JP, White J, Ganesan K, Rathod PK, Chiu DT (2003) A microfluidic model for single-cell capillary obstruction by *Plasmodium falciparum*-infected erythrocytes. *Proc Nat'l Acad Sci USA* 100:14618–14622.
2. Cranston HA, et al. (1984) *Plasmodium falciparum* maturation abolishes physiologic red cell deformability. *Science* 223:400–403.
3. Ho M, White NJ (1999) Molecular mechanisms of cytoadherence in malaria. *Am J Physiol* 276:C1231–C1242.
4. Brown H, et al. (1999) Evidence of blood-brain barrier dysfunction in human cerebral malaria. *Neuropath Appl Neuro* 25:331–340.
5. Ho M, Hickey MJ, Andonegui AG, Kubes P (2000) Visualization of *Plasmodium falciparum*-endothelium interactions in human microvasculature: mimicry of leukocyte recruitment. *J Exp Med* 192:1205–1211.
6. Dondorp AM, Pongponratn E, White N (2004) Reduced microcirculatory flow in severe falciparum malaria: pathophysiology and electron-microscopic pathology. *Acta Trop* 89:309–317.
7. Adams S, Brown H, Turner G (2002) Breaking down the blood-brain barrier: signaling a path to cerebral malaria? *Trends Parasitol* 18:360–366.
8. Antia M, Herricks T, Rathod PK (2007) Microfluidic modeling of cell-cell interactions in malaria pathogenesis. *PLoS Pathog* 3:939–945.
9. Roy S, Dharmadhikari JA, Dharmadhikari AK, Mathur D, Sharma S (2005) Plasmodium-infected red blood cells exhibit enhanced rolling independent of host cells and alter flow of uninfected red cells. *Curr Sci India* 89:1563–1570.
10. Cooke BM, et al. (1994) Rolling and stationary cytoadhesion of red blood cells parasitized by *Plasmodium falciparum*: separate roles for ICAM-1, CD36 and thrombospondin. *Brit J Haematol* 87:162–170.
11. Yipp BG, et al. (2000) Synergism of multiple adhesion molecules in mediating cytoadherence of *Plasmodium falciparum*-infected erythrocytes to microvascular endothelial cells under flow. *Blood* 96:2292–2298.
12. Pivkin IV, Karniadakis GE (2008) Accurate coarse-grained modeling of red blood cells. *Phys Rev Lett* 101:118105.
13. McWhirter JL, Noguchi H, Gompper G (2009) Flow-induced clustering and alignment of vesicles and red blood cells in microcapillaries. *Proc Nat'l Acad Sci USA* 106:6039–6043.
14. Fedosov DA, Caswell B, Karniadakis GE (2010) A multiscale red blood cell model with accurate mechanics, rheology, and dynamics. *Biophys J* 98:2215–2225.
15. Fedosov DA (2010) Multiscale modeling of blood flow and soft matter. PhD thesis (Division of Applied Mathematics, Brown University).
16. Quinn D (2010) Dynamic behavior of healthy and malaria infected human red blood cells. PhD thesis (Department of Mechanical Engineering, Massachusetts Institute of Technology).
17. Li J, Dao M, Lim CT, Suresh S (2005) Spectrin-level modeling of the cytoskeleton and optical tweezers stretching of the erythrocyte. *Biophys J* 88:3707–3719.
18. Hammer DA, Apte SM (1992) Simulation of cell rolling and adhesion on surfaces in shear flow: general results and analysis of selectin-mediated neutrophil adhesion. *Biophys J* 63:35–57.
19. King MR, Hammer DA (2001) Multiparticle adhesive dynamics: hydrodynamic recruitment of rolling leukocytes. *Proc Nat'l Acad Sci USA* 98:14919–14924.
20. Alon R, Hammer DA, Springer TA (1995) Lifetime of the P-selectin-carbohydrate bond and its response to tensile force in hydrodynamic flow. *Nature* 374:539–542.
21. Chen S, Springer TA (1999) An automatic braking system that stabilizes leukocyte rolling by an increase in selectin bond number with shear. *J Cell Biol* 144:185–200.
22. Park Y-K, et al. (2008) Refractive index maps and membrane dynamics of human red blood cells parasitized by *Plasmodium falciparum*. *Proc Nat'l Acad Sci USA* 105:13730–13735.
23. Suresh S, et al. (2005) Connections between single-cell biomechanics and human disease states: gastrointestinal cancer and malaria. *Acta Biomater* 1:15–30.
24. Maeda N, Suzuki Y, Tanaka J, Tateishi N (1996) Erythrocyte flow and elasticity of microvessels evaluated by marginal cell-free layer and flow resistance. *Am J Physiol* 271:H2454–H2461.
25. Kim S, Long LR, Popel AS, Intaglietta M, Johnson PC (2007) Temporal and spatial variations of cell-free layer width in arterioles. *Am J Physiol* 293:H1526–H1535.
26. Pries AR, Neuhaus D, Gaehtgens P (1992) Blood viscosity in tube flow: dependence on diameter and hematocrit. *Am J Physiol* 263:H1770–H1778.
27. Weinbaum S, Tarbell JM, Damiano ER (2007) The structure and function of the endothelial glycocalyx layer. *Annu Rev Biomed Eng* 9:121–167.
28. Popel AS, Johnson PC (2005) Microcirculation and hemorheology. *Annu Rev Fluid Mech* 37:43–69.
29. Springer TA (1995) Traffic signals on endothelium for lymphocyte recirculation and leukocyte emigration. *Annu Rev Physiol* 57:827–872.
30. Finger EB, et al. (1996) Adhesion through L-selectin requires a threshold hydrodynamic shear. *Nature* 379:266–269.
31. Haenscheid T (1999) Diagnosis of malaria: a review of alternatives to conventional microscopy. *Clin Lab Haematol* 21:235–245.
32. Wilkinson RJ, Brown JL, Pasvol G, Chiodini PL, Davidson RN (1994) Severe falciparum malaria: predicting the effect of exchange transfusion. *Q J Med* 87:553–557.
33. Hoogerbrugge PJ, Koelman JMVA (1992) Simulating microscopic hydrodynamic phenomena with dissipative particle dynamics. *Europhys Lett* 19:155–160.
34. Gompper G, Kroll DM (2004) *Statistical mechanics of membranes and surfaces*, eds DR Nelson, T Piran, and S Weinberg (World Scientific, Hackensack, NJ).